JOURNAL OF VIROLOGY, Dec. 1996, p. 8908–8916 Vol. 70, No. 12
0022-538X/96/$04.00+0

Brome Mosaic Virus Helicase- and Polymerase-Like Proteins Colocalize on the Endoplasmic Reticulum at Sites of Viral RNA Synthesis

MARÍA A. RESTREPO-HARTWIG AND PAUL AHLQUIST*

Institute for Molecular Virology, University of Wisconsin—Madison, Madison, Wisconsin 53706-1596

Received 28 June 1996/Accepted 27 August 1996

The helicase-like 1a and polymerase-like 2a proteins of brome mosaic virus (BMV) are required for viral RNA replication in vivo, are present in membrane-bound viral RNA polymerase extracts, and share conservation with the many other members of the alphavirus-like superfamily. To better understand BMV RNA replication and BMV-host interactions, we used confocal microscopy and double-label immunofluorescence to determine and compare the sites of 1a, 2a, and nascent viral RNA accumulation in BMV-infected barley protoplasts. 1a and 2a showed nearly complete colocalization throughout infection, accumulating in defined cytoplasmic spots usually adjacent to or surrounding the nucleus. These spots grew throughout infection and by 16 h postinoculation often assumed a vesicle-like appearance. The BMV RNA replication complex incorporated 5-bromouridine 5′-triphosphate into RNA in vitro and in vivo, allowing immunofluorescent detection of nascent RNA. The cytoplasmic sites of BMV-specific RNA synthesis coincided with the sites of 1a and 2a accumulation, and at the resolution of confocal microscopy, all sites of 1a and 2a accumulation were sites of BMV RNA synthesis. Double-label immunofluorescence detection of selected subcellular markers and 1a or 2a showed that BMV replication complexes were tightly associated with markers for the endoplasmic reticulum but not the medial Golgi or later compartments of the cellular secretory pathway. Defining this association of BMV RNA replication complexes with endoplasmic reticulum markers should assist in identifying and characterizing host factors involved in BMV RNA replication.

For most or all positive-strand RNA viruses of eukaryotes examined to date, the viral RNA-dependent RNA replication complex copurifies with membrane extracts from infected cells (4, 11, 16, 21, 45, 46, 55). In some cases, negative-strand RNA synthesis activity can be solubilized from such membrane extracts (55, 64), but in vitro studies with positive-strand RNA viruses as varied as picornaviruses and nodaviruses suggest that membrane association is important for synthesis of positive-strand RNA (3, 47, 64). For a number of positive-strand RNA viruses, RNA replication also has been implicated in infection-specific changes in the ultrastructure of membranes in various parts of the cellular secretory pathway (6, 19, 20, 29, 38, 48). Defining the mechanisms of positive-strand RNA virus RNA replication thus appears important for understanding infection pathology, as well as the basic life cycle, control, and beneficial uses of such viruses. However, at present neither the mechanisms of positive-strand RNA virus RNA replication nor the nature and function of its membrane association are well understood.

Brome mosaic virus (BMV), type member of the *Bromovirus* genus, is a positive-strand RNA virus in the alphavirus-like superfamily (1). The BMV genome is composed of three RNAs, designated RNA1 to RNA3. RNA3 encodes the 3a protein, which is required for cell-to-cell movement of BMV infection in its natural plant hosts, and the coat protein, which is translated from a subgenomic mRNA, RNA4. RNA1 and RNA2 encode nonstructural proteins 1a and 2a, respectively, which are essential RNA replication factors (17, 37). The 109-kDa 1a protein contains motifs conserved with m^7G methyltransferases and helicases, while the 94-kDa 2a protein has extensive similarities with RNA-dependent RNA polymerases (2, 28). 1a and 2a interact in vitro (36), and genetic studies show that compatible 1a-2a interaction is essential for RNA replication in vivo (15, 60). Recently it was shown that BMV RNA derivatives can replicate and express marker genes in the genetically tractable yeast *Saccharomyces cerevisiae* (33).

As first shown by Hall and colleagues, BMV-infected cells can be extracted to yield a membrane-bound, infection-specific, template-dependent, RNA-dependent RNA polymerase (RdRp) that selectively copies added BMV positive-strand RNAs into full-length negative-strand RNAs (8, 26, 46). After detergent solubilization, this BMV RdRp activity copurifies with an immunoprecipitable complex of 1a, 2a, and 5-6 host factors (55, 56). An equivalent, initially membrane-bound BMV RNA polymerase activity can be isolated from yeast expressing the BMV 1a and 2a proteins and replicating BMV RNA derivatives (54). Since 1a and 2a lack obvious membrane-spanning domains, the nature of their association with membranes in such complexes is not yet clear.

To better understand the roles and interaction of BMV RNA replication proteins 1a and 2a and their association with cell membranes, and to provide a cell biology context for interpreting the involvement of host factors that genetic studies may implicate in BMV RNA replication, we explored the localization of 1a and 2a in BMV-infected protoplasts from a natural BMV host, barley. Using high-resolution immunofluorescence confocal microscopy and new RNA labeling approaches, we compared the intracellular distributions of 1a, 2a, BMV RNA synthesis, and selected markers for relevant cell membrane compartments.

* Corresponding author. Mailing address: Bock Labs, 1525 Linden Dr., Madison, WI 53706-1596. Phone: (608) 263-5916. Fax: (608) 262-7414. Electronic mail address: Ahlquist@facstaff.wisc.edu.

MATERIALS AND METHODS

Cells and virus stocks. Isolation and inoculation of barley protoplasts (*Hordeum vulgare* L. cv Morex) were performed as previously described (39). Virions

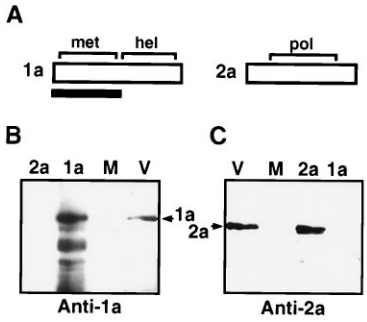

FIG. 1. (A) Schematic diagram of BMV proteins 1a (109 kDa) and 2a (94 kDa) (open boxes), showing the methyltransferase-like (met) and helicase-like (hel) domains of 1a and the polymerase-like (pol) domain of 2a (brackets). The portion of 1a (amino acids 1 to 502) that was expressed in *E. coli* and used to raise the anti-1a antiserum is indicated by the black bar beneath the protein representation. (B and C) Western blot analyses using anti-1a antiserum (B) and anti-2a IgG (C) (see Results). Lane 2a, insoluble fraction from 2a-expressing baculovirus-infected Sf21 insect cells; 1a, insoluble protein fraction from *E. coli* expressing full-length 1a; M, total SDS-soluble protein extracted from mock-inoculated barley protoplasts at 20 hpi; V, total SDS-soluble protein extracted from BMV virion-inoculated barley protoplasts at 20 hpi. Samples were loaded and electrophoresed, in the mirror image order shown, on a single 0.1% SDS–10% polyacrylamide gel, with prestained molecular weight markers (high-range SDS-PAGE standards; Bio-Rad) loaded in a single lane between the two panels shown. After electrophoresis, the proteins were transferred onto an Immobilon-P membrane, which was then sliced through the center of the lane containing the prestained molecular weight markers. The resulting two halves of the membrane were probed with either anti-1a antiserum or anti-2a IgG, as shown, and the bound antibodies were visualized by chemiluminescence. Before exposure to film, the membrane halves were realigned by using the visible, prestained molecular weight markers as guides. The positions of full-length 1a and 2a are indicated in the center.

were prepared from infected cells and transfected into protoplasts as described by Sakal et al. (59).

Antibodies. Mouse monoclonal immunoglobulin G's (IgGs) to 2a were a generous gift from Rick Hershberger. These antibodies were raised against 2a protein excised from a glutathione *S*-transferase–2a fusion polyprotein expressed in *Escherichia coli* and were purified by using protein A–Sepharose CL-4B columns (30). Anti-2a monoclonal antibody 10B3, which recognizes the polymerase-like domain, was used for most experiments, including all those represented in the figures. Occasionally, anti-2a monoclonal antibodies 13E2 and 6G12, which recognize the N terminus and the C terminus, respectively, were used with equivalent results (see Results). To prepare the antigen for anti-1a antiserum (Fig. 1A), site-directed mutagenesis (41) was used to create *Nde*I sites in full-length BMV RNA1 cDNA clone pB1TP3 (34) by adding the nucleotides CAT immediately before the 1a initiator ATG (creating pB1MR2) and then adding CATATG immediately after 1a codon 502 in pB1MR2. After confirmation of the sequence, the *Nde*I-*Nde*I fragment was isolated, purified, and inserted into *Nde*I-digested pET11a (Novagen), generating a plasmid, pB1MR6, giving isopropylthiogalactopyranoside (IPTG)-induced expression of 1a amino acids 1 to 502. pB1MR6 was transformed into *E. coli* BL21, 1a expression was induced with 0.5 mM IPTG, and the cells were grown further 3 h at 37°C, harvested, and lysed. The insoluble protein fraction, containing the 1a fragment, was isolated and electrophoresed on a 0.1% sodium dodecyl sulfate (SDS)–10% polyacrylamide gel, and the proteins were visualized by precipitation of SDS-protein complexes upon soaking the gel in 0.25% KCl. The IPTG-specific 1a band was excised, fragmented by repeated passage through a 22-gauge syringe needle, diluted in phosphate-buffered saline (PBS; 37.5 mM K_2HPO_4, 10 mM KH_2PO_4, 150 mM NaCl), and used for injecting a New Zealand White rabbit (27). The rabbit was injected intradermally with antigen-complete Freund's adjuvant emulsion, boosted subcutaneously 4 weeks later with the same emulsion, and boosted twice at 3-week intervals with antigen-incomplete Freund's adjuvant emulsion. Serum was isolated 2 weeks after the last boost. All animal procedures were performed at the Animal Care Unit of the University of Wisconsin—Madison Medical School.

Antisera to the tomato binding protein (BiP) and to a xyloglycan epitope were generous gifts from Maarten Chrispeels (unpublished results and reference 42, respectively). Antiserum to barley calreticulin was a kind gift from Fuqiang Chen (10).

Immunoblot analysis. Full-length 1a was expressed in *E. coli* from a pET11a-derived plasmid constructed by transferring the *Nde*I-*Nco*I fragment from pB1MR2, containing 1a codons 1 through 682, into *Nde*I-*Nco*I-cut pΔ502ET (35). Baculovirus-expressed full-length 2a has been described elsewhere (36). SDS-polyacrylamide gel electrophoresis (PAGE), transfer to an Immobilon-P membrane, probing with antibodies, and detection by chemiluminescence were performed essentially as described previously (36) except that the primary antibodies were used at 1:6,000 dilution and incubated with the blot for 1 h at room temperature.

Immunofluorescence staining. Protoplasts were harvested at the times indicated in the text and figures and processed for indirect immunofluorescence as described by van Lent et al. (61), with minor modifications. Briefly, the protoplasts were transferred to acid-washed, poly-L-lysine-coated slides, allowed to settle for 2 min, and fixed for 20 min in 96% ethanol at room temperature. To inhibit nonspecific antibody binding, cells were incubated 15 min in 5% bovine serum albumin (BSA) in PBS. Primary antibodies were diluted 1:100 in 1% BSA–0.05% Nonidet P-40 in PBS and incubated with the cells for 1 h at room temperature. After three washes with PBS, donkey anti-rabbit or anti-mouse secondary antibodies conjugated to fluorescein, lissamine rhodamine, or cyanine (Jackson Laboratories) were added at 1:100 dilution for 1 h at room temperature. After three washes with PBS, the slides were dried and coverslips were mounted with 60% glycerol containing 0.3% phenylenediamine. For nuclear staining, a 30-min incubation in propidium iodide (0.5 μg/ml) was added after secondary antibody treatment. Images were obtained for 0.5-μm optical sections by using a Bio-Rad MRC-600 or MRC-1000 confocal microscope and appropriate filters, saved in COMOS format, and processed on Macintosh computers using Adobe Photoshop software. To ensure examination of the full range of normal results in BMV infection, each experiment was performed 4 to 10 times. For each independent experiment and for each relevant test in that experiment, many cells were examined and images were recorded for 6 to 14 cells.

Labeling and detection of nascent RNA. BMV RdRp was isolated and solubilized as described previously (55). BMV RdRp assays using [α-^{32}P]CTP label were carried out as described previously (55) or with the substitution of 5-bromouridine 5′-triphosphate (BrUTP) for UTP. The resulting double-stranded RNA products were recovered by phenol extraction, treated with S1 nuclease to eliminate any nontemplated nucleotide additions by possible contaminating terminal transferase activity (55), separated by nondenaturing agarose gel electrophoresis, and visualized by exposing the dried gel to a PhosphorImager screen.

For in vivo labeling with BrUTP, cells were inoculated and incubated for the times indicated in the text, at which point 80% of the medium was removed and actinomycin D was added to 20 mM where indicated. After 60 min of further incubation at 30°C, BrUTP was added to 10 mM, and after 2 to 6 min more at room temperature, cells were transferred to poly-L-lysine-coated microscope slides, allowed to settle 2 min, fixed in 96% ethanol, and processed for indirect

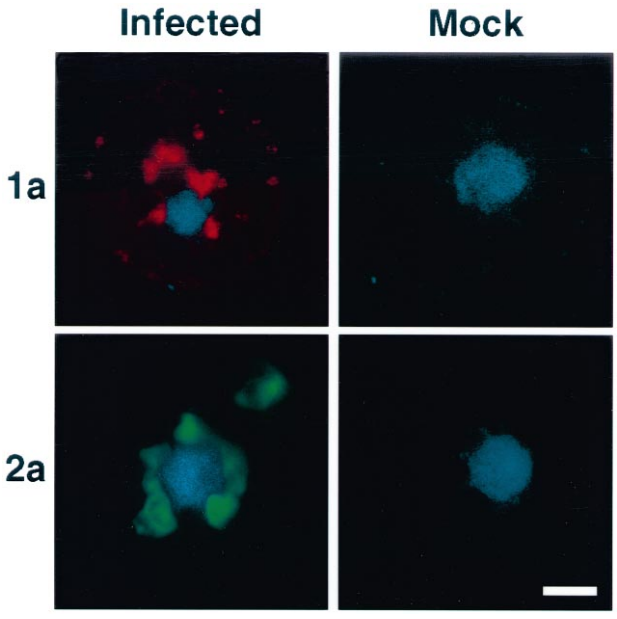

FIG. 2. Independent immunostaining of BMV-infected (left panels) or mock-inoculated (right panels) barley protoplasts for 1a and 2a. Each panel shows a separate, representative barley protoplast (approximately 20 to 25 μm in diameter), which fills most of the panel (see faint background in upper left panel). At 21 hpi, the protoplasts were processed for indirect immunofluorescence using either anti-1a antisera (top panels) or anti-2a IgG (bottom panels) as primary antibodies followed by appropriate secondary antibodies conjugated to a fluorescent tag; they then were stained with propidium iodide to visualize nuclear DNA. For each cell, the differentially fluorescing protein and nuclear DNA images were gathered separately from the same 0.5-μm optical section by using a confocal microscope and appropriate filters, and the two images were digitally superimposed to depict the distribution of 1a or 2a relative to the nucleus. Blue, DNA; red, 1a; green, 2a. Bar = 5 μm.

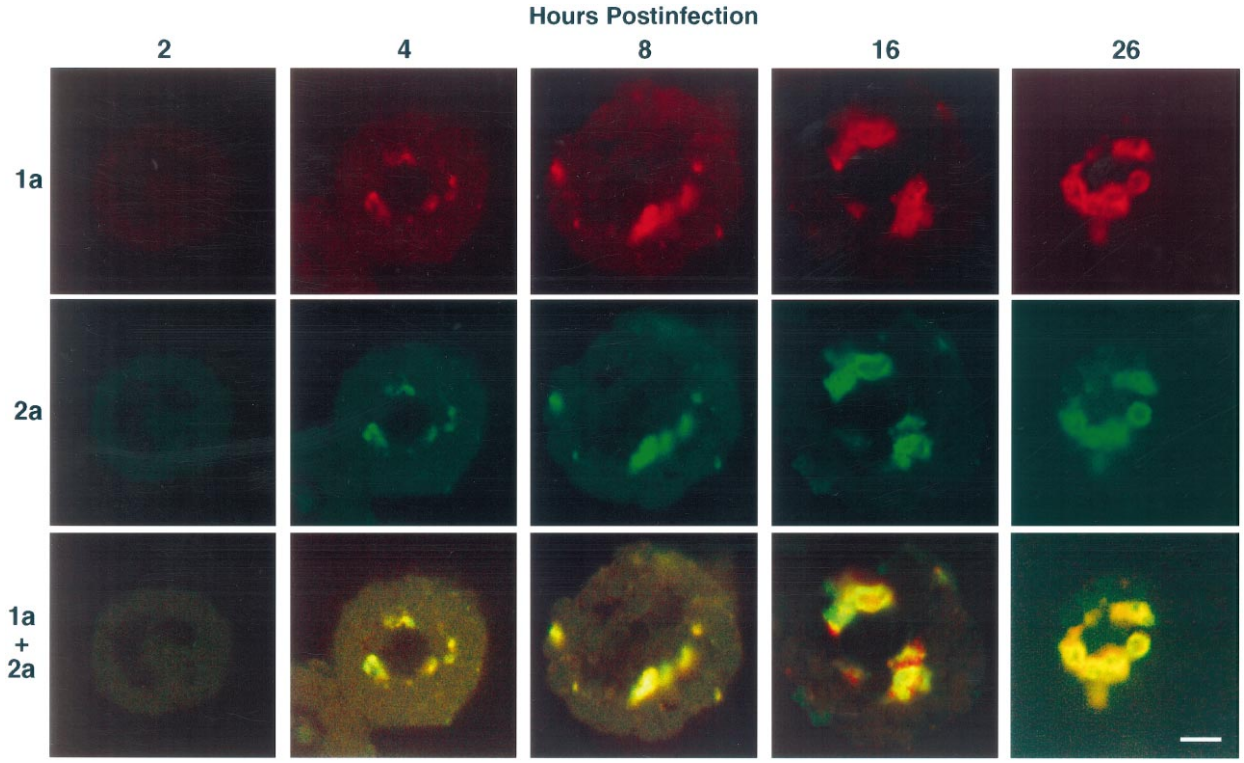

FIG. 3. Time course of 1a and 2a accumulation and colocalization in barley protoplasts. The five columns show representative images from five different BMV virion-inoculated protoplasts fixed at the indicated times after inoculation and processed for double-label immunofluorescence using anti-1a antisera and anti-2a IgG. Top row, 1a immunofluorescence (red); center row, 2a immunofluorescence (green) imaged in the same 0.5-μm optical section as 1a; bottom row, digital superposition of the 1a and 2a images, where colocalization of 1a and 2a signals produces yellow. Bar = 5 μm.

immunofluorescence as described above, using a primary antibody that detects incorporated BrUTP (32). For some samples, nascent RNA was removed by adding a 20-min treatment with RNase A (100 μg/ml) between cell fixation and immunostaining.

RESULTS

BMV 1a and 2a localize in cytoplasmic patches. To visualize the intracellular distribution of BMV RNA replication proteins 1a and 2a by immunofluorescence, we used a polyclonal rabbit antiserum raised against the N-terminal half of 1a (amino acids 1 to 502; Fig. 1A) (anti-1a) and a purified mouse monoclonal IgG preparation that recognized the central polymerase-like domain of 2a (anti-2a). As shown in Fig. 1B, anti-1a recognized *E. coli*-expressed full-length 1a and a number of 1a degradation products in the *E. coli* extract (lane 1a). Anti-1a also recognized a protein of full-length 1a mobility in extracts from BMV virion-inoculated barley protoplasts (lane V) but did not cross react with baculovirus-expressed 2a (lane 2a). Conversely, as shown in Fig. 1C, anti-2a recognized baculovirus-expressed 2a (lane 2a) and a protein of the same mobility in the extract from BMV virion-inoculated protoplasts (lane V) but did not cross-react with 1a (lane 1a). Neither anti-1a or anti-2a reacted with proteins extracted from mock-inoculated protoplasts (lanes M).

To obtain populations of efficiently and synchronously infected cells, leaf mesophyll protoplasts from barley, a natural BMV host, were isolated and infected with BMV virions. After 21 h of incubation, the protoplasts were harvested, fixed, and processed for indirect immunofluorescence using either anti-1a or anti-2a. To visualize the nucleus, the cells were stained with propidium iodide, a fluorescent intercalator of DNA. Double-label fluorescence images of 1a or 2a and nuclear DNA were then collected by using a confocal microscope to image optical sections with a focal depth of only 0.5 μm, thus removing out-of-focus glare and improving resolution (63). As illustrated by the representative examples in Fig. 2, 1a (colorized red, upper left panel) and 2a (colorized green, lower left panel) each appeared in defined spots in the cytoplasm of infected cells. Many, but not all, of these spots closely surrounded the nucleus, as revealed by DNA staining (colorized blue). Uninfected cells processed and imaged in parallel showed equivalent nuclear DNA staining, but no signal was seen for either anti-1a (upper right panel) or anti-2a (lower right panel). In addition to the anti-1a and anti-2a antibodies described above, two other anti-2a monoclonal antibodies and a polyclonal serum to the C-terminal 460 amino acids of 1a (which do not overlap the N-terminal 1a region expressed above) were also used in immunofluorescence microscopy of BMV-infected and mock-inoculated cells, yielding results equivalent to those shown in Fig. 2.

1a and 2a largely colocalize throughout infection. Because 1a and 2a coprecipitate from BMV replication complex preparations (55, 57), interact in vitro (35, 36), and function interdependently in vivo (15), it seemed likely that at least portions of the 1a and 2a populations would colocalize. To examine this possibility, we fixed cells at different times postinoculation and performed double-label indirect immunofluorescence with anti-1a and anti-2a, visualized with rhodamine- and fluorescein-conjugated secondary antibodies, respectively. Representative images from cells harvested at five different times postinoculation are shown in Fig. 3. Each column presents three images from the same focal plane of a cell harvested at the indicated time: the top panel shows 1a immunofluorescence (colorized red), the center panel shows 2a immunofluorescence (colo-

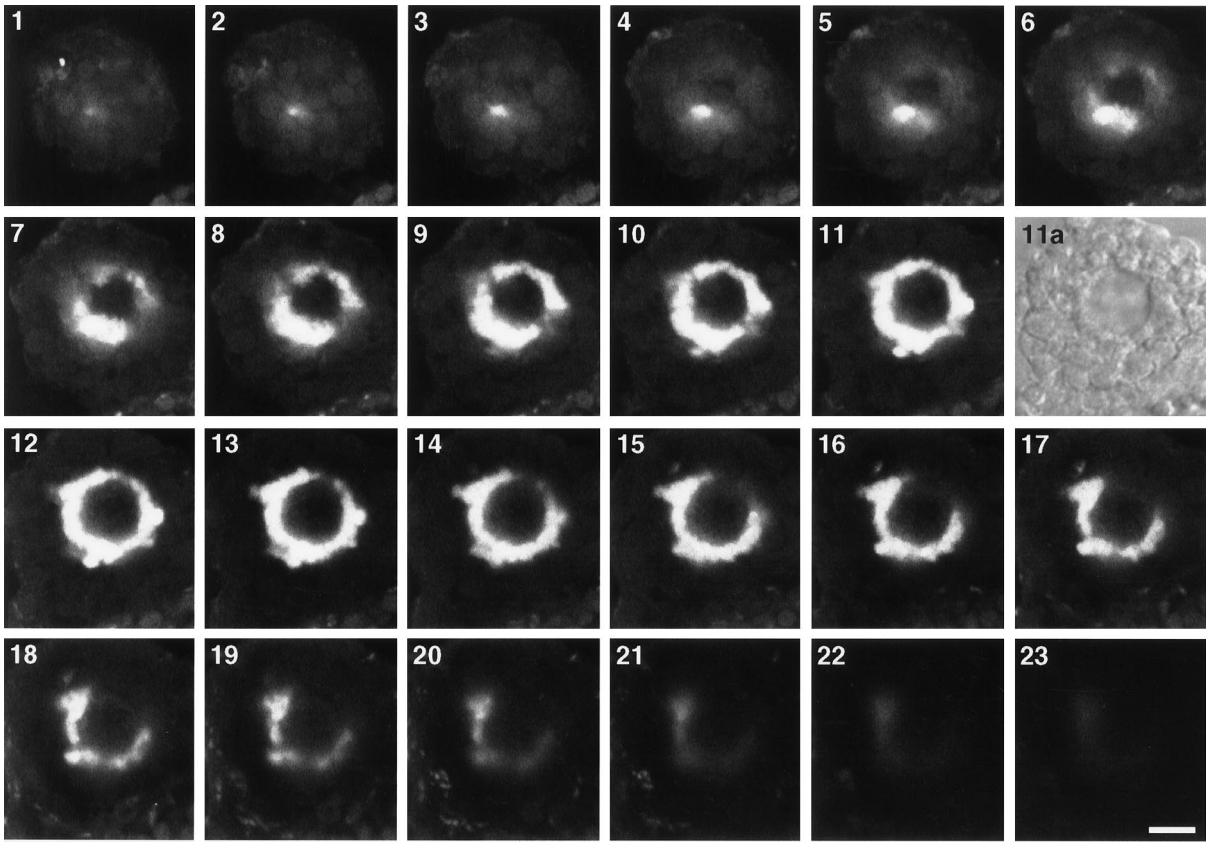

FIG. 4. Distribution of 2a throughout a representative BMV-infected protoplast. Immunofluorescence images were gathered for consecutive optical sections spaced every 0.5 μm through a BMV-infected protoplast that had been fixed at 21 hpi and immunostained for 2a. The images shown correspond to the sequential optical sections in which 2a immunofluorescence was detected. As an aid to visualizing the protoplast, panel 11a shows a Nomarski image of the same optical section as panel 11. Bar = 5 μm.

rized green), and the bottom panel shows the superposition of 1a and 2a signals. At 4 h postinfection (hpi), 1a and 2a were both visible in cytoplasmic spots near the nucleus. The size of these immunofluorescent structures increased with time, and by 16 to 26 hpi, they often appeared as vesicle-like structures (Fig. 3).

As shown in the bottom panels of Fig. 3, digital superposition of the colorized 1a and 2a fluorescence images allows fine comparisons, since colocalization of red and green signals in a single pixel produces yellow, while separated signals remain red or green. At all time points, such superposition revealed nearly complete colocalization of 1a and 2a. While the generally coincident relation of 1a and 2a was apparent throughout Fig. 3, some differences in the fine structure of 1a and 2a signal distributions could sometimes be noted in high-resolution images (e.g., 16-hpi images in Fig. 3). Whether this reflected real differences in the localization of minor portions of the 1a and 2a populations or occasional imperfections in detecting the full extent of each protein population is not yet clear.

Serial optical sectioning of 1a and 2a distribution. The distribution of 1a and 2a throughout the cell was further analyzed by imaging successive confocal optical sections, spaced at 0.5-μm intervals, through individual infected cells. In the representative example shown in Fig. 4, a cell was fixed at 21 hpi and processed for indirect immunostaining using anti-2a. 2a staining was visible in at least 22 contiguous optical sections of the cell, corresponding to a region of 11-μm thickness in the center of this approximately 25-μm diameter cell.

Beginning at one edge of this region in image 1, 2a appeared first in a small discrete spot. In successively deeper focal planes of the cell (images 2 to 11), this spot grew to form an initially fragmented and then complete ring, whose diameter expanded through the succeeding sections to approximately 8 to 9 μm. The circular region enclosed by 2a was also clearly visible in superimposable Nomarski images of the same sections (compare images 11 and 11a) and appears to correspond to the nucleus, as determined by comparison of Nomarski imaging and nuclear DNA staining of other cells, and on double-label imaging of 2a and nuclear DNA as in Fig. 2. In successively deeper focal planes (images 12 to 14), 2a initially continued to ring the nucleus, with some protrusions emanating away from this central ring into the cytoplasm. In deeper optical sections (images 15 to 23), 2a extended over only part of the nuclear circumference, yielding an increasingly fragmented semicircle. By images 19 to 23, the intensity of the 2a signal was probably also reduced by photobleaching as a result of the repeated laser scanning used to produce images 1 to 18.

Together, the serial images in Fig. 4 indicate that 2a was distributed around a portion of the outer nuclear surface, forming an irregularly bounded girdle or crown with some protrusions away from the nucleus. Serial optical sections were also gathered for protoplasts immunostained for 1a, or for 1a and 2a, with results similar to those in Fig. 4. In most or all cells examined closely, at least a portion of the 2a and 1a distributions were associated with the nuclear boundary. However, in some sections of some cells, protrusions of the 1a and 2a distribution into the cytoplasm, or sites of 1a and 2a accumulation well separated from the nucleus, were much more prom-

inent than in Fig. 4 (see Fig. 2, 3, and 5 to 7). This distribution of perinuclear sites with cytoplasmic extensions is consistent with additional results, shown below, indicating that 1a and 2a colocalize with markers of the endoplasmic reticulum (ER). Figure 4 also illustrates that since each confocal image represents a single, narrow optical section or plane from a cell, the 2a and 1a pattern visualized from a given cell can vary dramatically according to the focal plane selected and the rotational orientation of the cell with respect to the focal plane.

BrUTP incorporation by BMV RNA replication complex in vitro and in vivo. We were interested in determining whether any or all sites of 1a and 2a accumulation were also sites of RNA synthesis. [^{3}H]uridine has been used to label in vivo sites of RNA synthesis for some positive-strand RNA viruses, including Semliki Forest virus, poliovirus, and broad bean mottle virus (7, 14, 24). However, present [^{3}H]uridine detection methods are cumbersome and incompatible with simultaneous immunofluorescence detection of other markers such as viral proteins. In a recent alternate approach, nascent RNA transcribed in the nucleus from human or adenovirus DNA has been labeled with the nonradioactive UTP analog BrUTP and visualized by indirect immunofluorescence, allowing double-label comparisons with the distributions of other factors (32, 53).

The ability of the BMV replication complex to incorporate BrUTP into viral RNA was first tested in vitro, using a BMV RdRp extract able to synthesize negative-strand RNA from added BMV positive-strand RNAs (46, 55, 56; see also the introduction). Reaction mixtures contained BMV RdRp extract, added BMV virion RNA1 to RNA4 as templates, ATP, GTP, [α-^{32}P]CTP, and either UTP or BrUTP. After 60 min at 30°C, RNA products were recovered, separated by gel electrophoresis, and visualized by exposing the dried gel to a PhosphorImager screen to allow quantitative analysis. When RdRp assays were performed in the presence of UTP, prominent full-length negative-strand RNA products were detected for all four BMV RNAs (Fig. 5A, lane UTP). Replacing UTP with BrUTP resulted in essentially the same levels of viral RNA products as UTP (Fig. 5A, lane BrUTP): in Fig. 5A and similar experiments, total incorporation was 95 to 128% of that with UTP. When added UTP or BrUTP was omitted (Fig. 5A, lane −), only small amounts of labeled RNA (less than 4% of that made with added UTP or BrUTP) were synthesized, possibly by using residual UTP in the BMV RdRp extract. Thus, in vitro, BMV RdRp can incorporate BrUTP nearly as efficiently as UTP into full-length BMV RNA products.

To determine whether BMV RdRp incorporated BrUTP in vivo, BMV-infected or mock-inoculated cells were incubated for 4 to 8 min in the presence of BrUTP, immediately fixed, and processed for indirect immunofluorescence using a primary antibody that detects bromouridine-containing RNA (32). In mock-inoculated cells, a fluorescent signal was observed only in the nucleus (Fig. 5B, upper left panel). In infected cells, similar nuclear staining was seen together with stronger staining in cytoplasmic patches, primarily adjacent to the nucleus (Fig. 5B, upper right panel).

To further distinguish the sites of host transcription from those of infection-specific RNA synthesis, cells were incubated with actinomycin D, which blocks host DNA-dependent transcription without affecting BMV-directed, RNA-dependent RNA synthesis (43). As expected, when cells were preincubated with actinomycin D for 60 min prior to BrUTP addition, no nuclear signal was observed in either mock-inoculated or BMV-infected cells, but the strong cytoplasmic signals present in BMV-infected cells were unaffected (Fig. 5B).

Colocalization of RNA synthesis with 1a and 2a. To test the possible relationship between the sites of infection-specific RNA synthesis and the sites of 1a and 2a accumulation, BMV-infected cells were incubated for 8 min in the presence of BrUTP, fixed, and analyzed by double-label immunofluorescence using antibodies that recognize 1a and bromouridine-containing RNA. Representative results are shown in Fig. 6A, where each column presents three images of a single focal plane in a separate infected cell tested at 20 hpi: the top panel shows 1a immunofluorescence (colorized red), the center image shows BrUTP-labeled RNA immunofluorescence (colorized green), and the bottom image shows the superimposition of both. As illustrated, there was a striking coincidence between the distribution of 1a and BrUTP-labeled RNA. Similar results were observed when the cells were sequentially probed with mouse anti-2a, rhodamine-conjugated donkey anti-mouse antiserum, and a fluorescein-conjugated mouse antibody that recognizes bromouridine-containing RNA.

Prior immunofluorescence studies of BrUTP-labeled DNA-dependent transcription (22, 32, 53, 62) and the absence of BrUTP signal in mock-inoculated cells preincubated with ac-

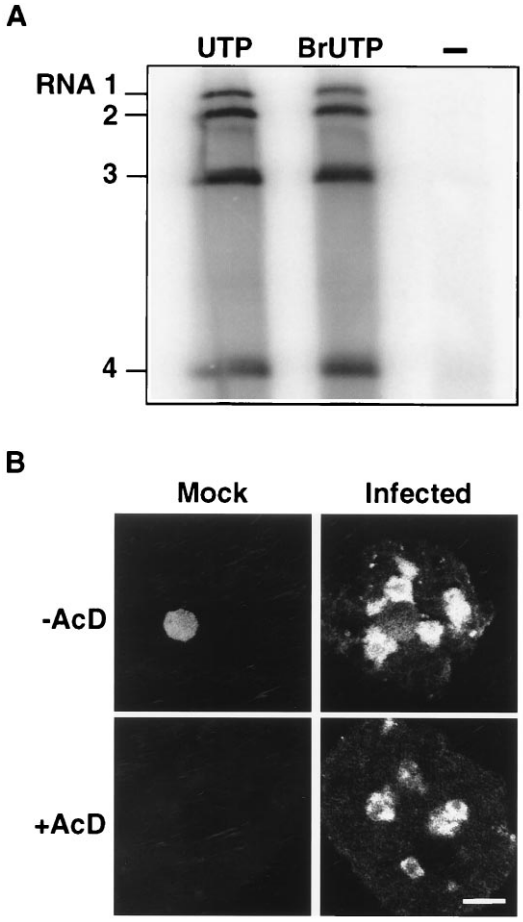

FIG. 5. In vitro and in vivo incorporation of BrUTP by the BMV RNA replication complex. (A) Autoradiograph of a nondenaturing 1% agarose gel showing the electrophoretic mobility of negative-strand RNA products synthesized in vitro by BMV RdRp extract on added BMV virion RNA1 to RNA4 templates in the presence of ATP, GTP, [α-^{32}P]CTP, and either UTP (left lane), BrUTP (center lane), or no added UTP (right lane). The positions of the BMV RNA1 to RNA4 products (which hybridize to the positive-strand template RNAs and so migrate as double-stranded RNAs) are indicated on the left. (B) Representative images from mock-inoculated (left panels) or BMV-infected (right panels) barley protoplasts incubated for 20 hpi, then incubated an additional hour with (bottom panels) or without (top panels) actinomycin D, labeled for 8 min with BrUTP, fixed, and processed for indirect immunostaining with an antibody that recognizes incorporated BrUTP. Bar = 5 μm.

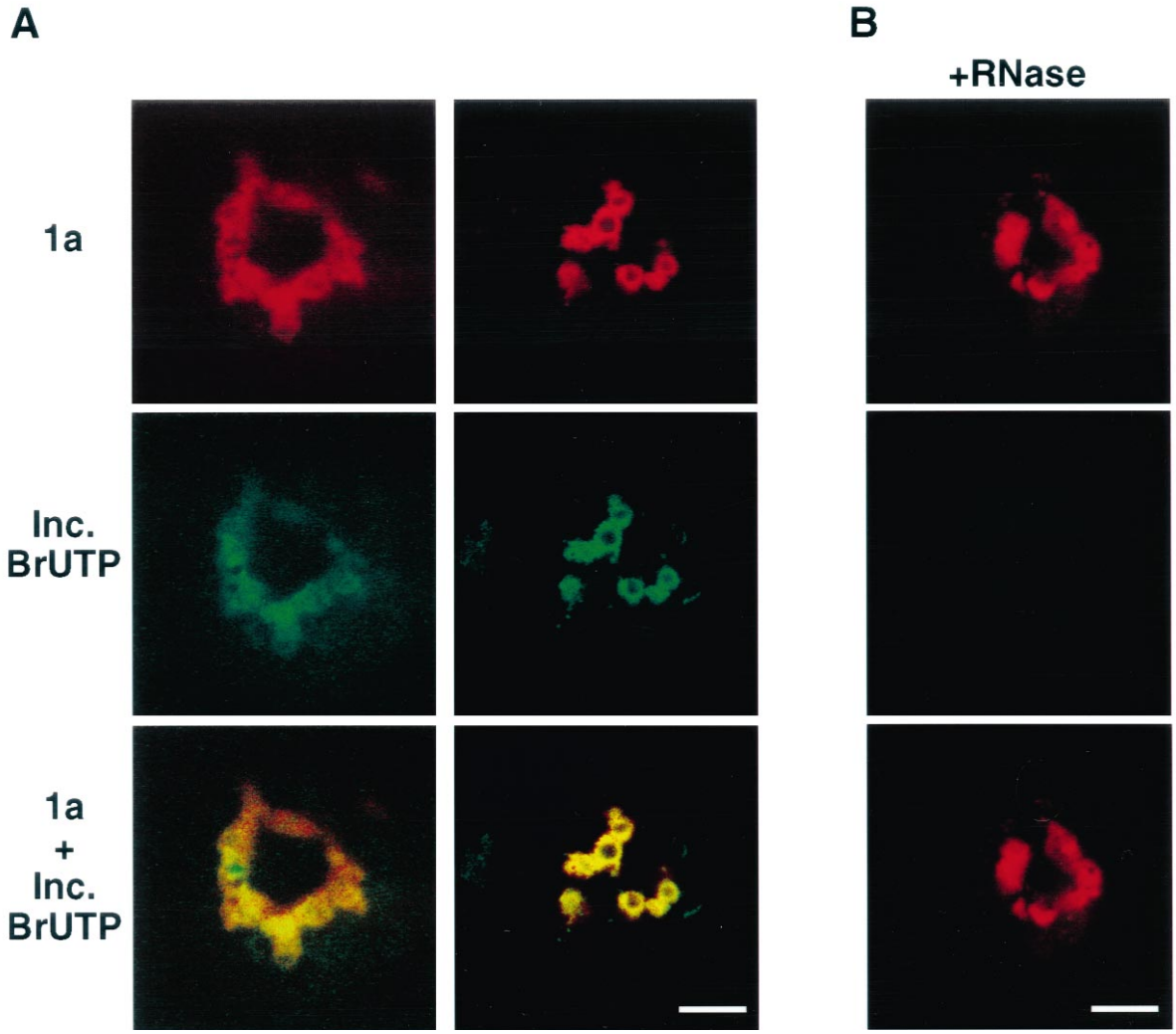

FIG. 6. Colocalization of incorporated BrUTP with 1a and RNase sensitivity of the incorporated BrUTP signal. (A) The two columns show images from two different, representative BMV-infected protoplasts incubated for 20 hpi, then labeled for 8 min with BrUTP, fixed, and processed for double label immunofluorescence using antibodies that detect 1a and incorporated BrUTP. Top row, 1a (red); center row, incorporated BrUTP (green) imaged in the same 0.5-μm optical section as 1a; bottom row, digital superposition of 1a and incorporated BrUTP. (B) Representative images from a BMV-infected protoplast processed as for panel A except that RNase A was added after fixation and before immunostaining. Bar = 5 μm.

tinomycin D (Fig. 5B) indicated that unincorporated BrUTP was not detected by the antibody and immunofluorescence protocol used for Fig. 5 and 6. To further confirm that the BrUTP labeling sites visualized in BMV-infected cells represented BrUTP incorporated into nascent viral RNA and not, e.g., BrUTP bound to BMV replication complexes, infected cells were treated with RNase A after incubation with BrUTP and fixation and before immunostaining. After such RNase treatment, 1a detection was unaffected (Fig. 6, right column, top panel), but no BrUTP signal could be detected (Fig. 6, right column, middle panel). Thus, the infection-specific immunofluorescence signal resulting from incubating cells with BrUTP represents labeling of RNA.

BMV 1a and 2a colocalize with ER markers. As noted above, the perinuclear/cytoplasmic distribution of 1a and 2a suggested a possible relation with the ER. To test for association of BMV replication complexes with one or more membrane compartments of the cellular secretory apparatus, we performed double-label immunofluorescence using anti-1a or anti-2a together with antibodies to ER-resident proteins or to a xyloglycan epitope found in the *trans*-Golgi and later parts of the secretory pathway (Fig. 7).

As markers for the ER, we used antibodies to the binding protein BiP from tomato and to calreticulin from barley. BiP is an abundant ER lumenal protein involved in folding and assembly of new proteins in the ER (23). BiP is strongly conserved among eukaryotes, including mammals, plants, and yeasts (13, 49, 58), and is widely used as an ER marker (23, 25, 51). Calreticulin is a predominantly ER-localized calcium-binding protein whose sequence is also highly conserved across eukaryotes (50). Among other studies indicating a chiefly ER localization for calreticulin in many cell types, prior fluorescence microscopy studies of tobacco cells indicated that the major sites of calreticulin accumulation correspond to those of BiP (12). Representative optical sections from two different BMV-infected cells stained for BiP and 2a, and from two separate BMV-infected cells stained for calreticulin and 2a, are shown in Fig. 7A. BiP immunostaining (colorized green) revealed partial outlining of the nuclear envelope and cytoplasmic patches or vesicles, some of which were usually adja-

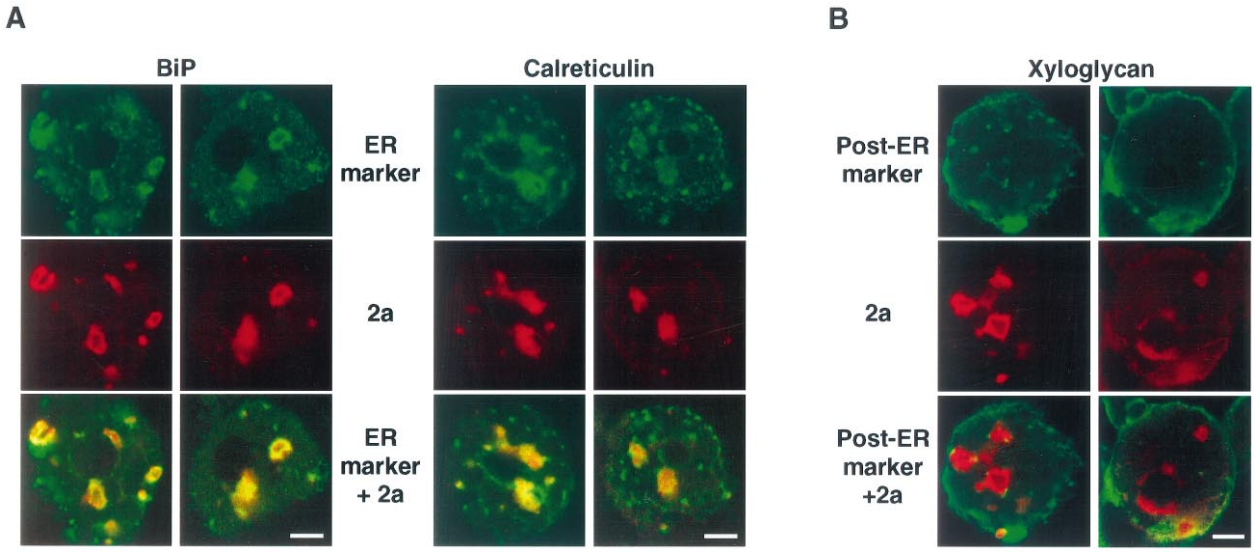

FIG. 7. ER association of BMV 1a and 2a. Each column shows images from a different, representative BMV-infected protoplast fixed at 20 hpi and treated for double-label immunofluorescence using anti-2a IgG and antibodies to ER-resident proteins calreticulin or BiP (ER markers) (A) or a xyloglycan epitope added to proteins in the *trans*-Golgi (post-ER marker) (B). Top row, immunofluorescence signal for the relevant cellular marker (green); center row, 2a immunofluorescence (red) imaged in the same 0.5-μm optical section; bottom row, digital superposition of the 2a and relevant cellular marker distributions. Bar = 5 μm.

cent to the nucleus (upper panels, left two columns in Fig. 7A and similar experiments). Calreticulin immunostaining (colorized green) revealed similar perinuclear and cytoplasmic structures but also included additional punctate sites of immunofluorescence in the cytoplasm (upper panels, right two columns in Fig. 7A and similar experiments). These additional punctate sites might arise as a result of localization of a fraction of calreticulin outside the ER or cross-reaction of the calreticulin antiserum with another factor. Alternatively, since barley protoplasts were analyzed, the anti-barley calreticulin antiserum used might provide more sensitive detection than the anti-tomato BiP antiserum. BiP and calreticulin immunofluorescence patterns were also examined for uninfected barley protoplasts but revealed no consistent, significant variations from the BiP and calreticulin patterns seen for infected cells in Fig. 7A and other experiments (see also Discussion).

As in previous figures, 2a immunostaining (colorized red) revealed cytoplasmic patches or vesicle-like structures (Fig. 7A, middle row). When the green-colorized BiP or calreticulin distributions and red-colorized 2a distributions from the same cell sections were superimposed (Fig. 7A, bottom row), the resulting yellow regions showed that the structures within which 2a accumulated also corresponded to sites of BiP and calreticulin accumulation. Nearly all of the large (>1.5-μm diameter) patches or vesicles stained by anti-BiP or anti-calreticulin antiserum also stained with anti-2a. However, only a few of the smaller (<1-μm diameter), punctate sites of calreticulin immunofluorescence showed 2a immunofluorescence (Fig. 7A, left two columns).

To compare the localization of the BMV RNA replication apparatus to post-ER compartments in the secretory pathway, we used an antibody against a xyloglycan epitope that is added to proteins in the medial Golgi and is found in this and later parts of the secretory pathway (42, 65, 66). Xyloglycan immunostaining primarily localized to the cell perimeter, to ovoid or fan-shaped structures adjacent to the cell perimeter, and to occasional distinct spots in the cytoplasm (Fig. 7B, top row, and similar experiments). In contrast, anti-2a immunofluorescence in the same focal planes revealed completely different patterns (Fig. 7B, middle row, and similar experiments), consistent with previously observed 2a distributions. When the green-colorized xyloglycan distributions and red-colorized 2a distributions from the same focal planes were superimposed (Fig. 7B, bottom row), little if any colocalization was visible. In some regions, the immunofluorescent signals of 2a and xyloglycan were in close proximity (e.g., Fig. 7B, lower right panel, lower edge of the cell), consistent with the interactive relation of the ER and Golgi apparatus. However, even in these regions, the red 2a and green xyloglycan signals remained almost completely distinct and there was a nearly total absence of the yellow signal of red/green superposition that was so prominent in Fig. 7A.

DISCUSSION

The 1a protein, which contains putative RNA capping and helicase domains, and the polymerase-like 2a protein are the only BMV-encoded proteins necessary for viral RNA replication and transcription. In this study, we used immunofluorescence confocal microscopy to show that the sites of 1a accumulation, 2a accumulation, and BMV RNA synthesis are all tightly associated in infected cells and highly localized with respect to cell architecture.

Colocalization of 1a, 2a, and BMV-specific RNA synthesis. Throughout infection, 1a and 2a were localized to distinct cytoplasmic sites in infected cells (Fig. 2). Consistent with in vivo genetic and in vitro biochemical results indicating that 1a and 2a interact (15, 35, 36, 55), the 1a and 2a distributions showed a high degree of colocalization (Fig. 3). This colocalization was not an artifact of the detection methods, since similar patterns were obtained when 1a and 2a were visualized independently by single-label immunofluorescence or simultaneously by double-label immunofluorescence, when antibodies against other regions of 1a or 2a were substituted, and when fluorescent tags were exchanged between 1a and 2a.

To visualize the sites of BMV RNA synthesis, we adapted BrUTP-labeling and detection approaches previously used to identify nuclear sites of DNA-dependent RNA transcription (32). In vitro, BMV RdRp incorporated BrUTP as readily as UTP into full-length viral RNA products, and, in vivo, BMV

directed cytoplasmic, infection-specific and actinomycin D-insensitive incorporation of BrUTP into RNase-sensitive products. Continued nuclear transcription in BMV-infected cells was not unexpected since BMV infection does not inhibit host protein synthesis (37). Nevertheless, in keeping with the high level of BMV RNA accumulation in infected cells (18), BMV-specific cytoplasmic BrUTP incorporation in cells infected for 18 to 21 h was much stronger than nuclear BrUTP incorporation (Fig. 5B).

Double-label immunofluorescence showed that the cytoplasmic sites of BMV-specific RNA synthesis corresponded closely to the sites of 1a and 2a accumulation. The nearly total coincidence of BrUTP and 1a or 2a signals over the intricate patterns observed (Fig. 6) showed that, at least at the resolution of confocal microscopy and at later stages of infection (ca. 20 hpi), virtually all sites of 1a and 2a accumulation were sites of active RNA synthesis. However, although the general colocalization was striking, minor differences were occasionally observed in the distributions of 1a, 2a, and BrUTP incorporation. As noted above, these variations might result from real differences in distribution or occasional imperfections in detection. For example, in the generally yellow pattern of 1a-BrUTP superposition in the bottom left panel in Fig. 6A, a single green spot reveals a site where the fluorescence signal for BrUTP incorporation was detected in the absence of a corresponding 1a signal. Since mutational analysis shows that 1a is required for all forms of BMV RNA synthesis (40), this may reflect a flaw in visualizing either the 1a or incorporated BrUTP pattern. Alternatively, it might reflect movement of some RNA product from its site of synthesis, although to minimize such movement, BrUTP labelling was carried out for only 4 to 8 min and the rest of the incorporated BrUTP remained superimposed with 1a.

Association of BMV RNA replication complexes with the ER. 1a and 2a accumulated in cytoplasmic patches that increased in size during infection and often assumed a vesicular appearance (Fig. 2 to 6). Most of these patches were adjacent to the nucleus, and by late infection in some cells, the 1a-2a distribution enveloped much of the nuclear surface, with some protrusions farther into the cytoplasm (Fig. 4). As suggested by this pattern, double-label immunofluorescence showed that all sites of 1a and 2a accumulation corresponded to sites of the ER markers BiP and calreticulin, and by late infection, most sites of BiP accumulation were also occupied by 1a and 2a (Fig. 7A). Complementing these results, there was no overlap between the distribution of 2a and that of a xyloglycan marker for the post-ER compartments of the secretory apparatus (Fig. 7B), confirming that little or none of the BMV replication complex passed from the ER into the *trans*-Golgi or the rest of the secretory pathway.

The association of 1a and 2a with the ER is consistent with the membrane association of BMV RdRp in extracts of infected cells (26, 55). At the resolution of confocal microscopy, no gross variations were evident in the distribution of ER (BiP and calreticulin) or post-ER (xyloglycan) markers in BMV-infected cells (Fig. 7) compared with uninfected cells (results not shown). However, prior electron microscope studies of bromovirus-infected leaf tissue and protoplasts reported dilation and/or proliferation of ER membranes near the nucleus and increased numbers of 50- to 100-nm cytoplasmic membrane vesicles that were suggested to arise from the ER (9, 38, 44). Because of a lack of specific probes for viral or host factors, these early studies were not able to define the relationship of these membrane effects to any specific BMV components or infection processes, nor were they able to conclusively establish the ER origin of the vesicles. Our results suggest that such changes may occur in conjunction with the ER-associated accumulation of 1a and 2a and synthesis of BMV RNA, although further high-resolution studies will be required to establish the ultrastructure of the sites of 1a and 2a accumulation and BMV RNA synthesis and their relationship to any specific membrane changes.

Poliovirus RNA synthesis has also been associated with vesicles that appear to be derived from dilated ER (5). However, the nonstructural proteins and RNA replication complexes of the alphaviruses, which are much more closely related to BMV than is poliovirus, have been localized to the surface of modified endosomes and lysosomes (20, 52). Thus, different members of the alphavirus-like superfamily appear to carry out RNA replication on different membrane sites or subsets of the cellular secretory and endocytosis pathways. This localization specificity underscores that targeting and assembly of the RNA replication complexes of these viruses must involve selective interaction of one or more viral replication factors with particular host factors, while the use of functionally distinct membranes by related viruses has implications about the type of contributions that membrane association makes to RNA replication. Among other possibilities consistent with varied membrane sites, membrane association might play a primarily structural or organizational role in the replication complex and/or allow exploitation of a class of enzymatic functions associated with multiple types of cytoplasmic membranes. Further investigation of the nature of virus-host interactions in BMV RNA synthesis and the structure of the RNA replication complex should be helpful in addressing these issues and defining the mechanisms of replication complex assembly and function. In turn, the definition of the ER as the site of 1a and 2a accumulation and action should assist in interpreting the results of yeast genetic studies identifying host genes whose function is required for BMV RNA synthesis (31, 33).

ACKNOWLEDGMENTS

We thank Fuqiang Chen for antisera to barley calreticulin and Maarten Chrispeels for antiserum to BiP and to the xyloglycan epitope.

This work was supported by the National Institutes of Health under grants GM35072 and GM51301. Confocal microscopy was performed at University of Wisconsin—Madison in the Keck Neural Imaging Laboratory and in the Integrated Microscopy Resource for Biomedical Research, which is supported in part by National Institutes of Health Biomedical Technology Grant RR00570.

REFERENCES

1. **Ahlquist, P.** 1992. Bromovirus RNA replication and transcription. Curr. Opin. Genet. Dev. **2:**71–76.
2. **Ahlquist, P., E. G. Strauss, C. M. Rice, J. H. Strauss, J. Haseloff, and D. Zimmern.** 1985. Sindbis virus proteins nsP1 and nsP2 contain homology to nonstructural proteins from several RNA plant viruses. J. Virol. **53:**536–542.
3. **Barton, D. H., and J. B. Flanegan.** 1993. Coupled translation and replication of poliovirus RNA in vitro: synthesis of functional 3D polymerase and infectious virus. J. Virol. **67:**822–831.
4. **Barton, D. J., S. G. Sawicki, and D. L. Sawicki.** 1991. Solubilization and immunoprecipitation of alphavirus replication complexes. J. Virol. **65:**1496–1506.
5. **Bienz, K., D. Egger, and L. Pasamontes.** 1987. Association of polioviral proteins of the P2 genomic region with the viral replication complex and virus-induced membrane synthesis as visualized by electron microscopic immunocytochemistry and autoradiography. Virology **160:**220–226.
6. **Bienz, K., D. Egger, T. Pfister, and M. Troxler.** 1992. Structural and functional characterization of the poliovirus replication complex. J. Virol. **66:**2740–2747.
7. **Bienz, K., D. Egger, Y. Rasser, and W. Bossart.** 1980. Kinetics and location of poliovirus macromolecular synthesis in correlation to virus-induced cytopathology. Virology **100:**390–399.
8. **Bujarski, J. J., S. F. Hardy, W. A. Miller, and T. C. Hall.** 1982. Use of dodecyl-β-D-maltoside in the purification and stabilization of RNA polymerase from brome mosaic virus-infected barley. Virology **119:**465–473.

9. **Burgess, J., F. Motoyosi, and E. N. Fleming.** 1974. Structural changes accompanying infection of tobacco protoplasts with two spherical viruses. Planta **117:**133–144.
10. **Chen, F., P. M. Hayes, D. M. Mulrooney, and A. Pan.** 1994. Identification and characterization of cDNA clones encoding plant calreticulin in barley. Plant Cell **6:**835–843.
11. **de Graaff, M., L. Coscoy, and E. M. Jaspars.** 1993. Localization and biochemical characterization of alfalfa mosaic virus replication complexes. Virology **194:**878–881.
12. **Denecke, J., L. E. Carlsson, S. Vidal, A.-S. Höglund, B. Ek, M. J. van Zeijil, K. C. Sinjorgo, and E. T. Palva.** 1995. The tobacco homolog of mammalian calreticulin is present in protein complexes in vivo. Plant Cell **7:**391–406.
13. **Denecke, J., M. H. S. Goldman, J. Demolder, J. Seurinck, and J. Botterman.** 1991. The tobacco luminal binding protein is encoded by a multigene family. Plant Cell **3:**1025–1035.
14. **de Zoeten, G. A., and D. E. Schlegel.** 1967. Nucleolar and cytoplasmic uridine-^{3}H incorporation in virus-infected plants. Virology **32:**416–427.
15. **Dinant, S., M. Janda, P. A. Kroner, and P. Ahlquist.** 1993. Bromovirus RNA replication and transcription require compatibility between the polymerase- and helicase-like viral RNA synthesis proteins. J. Virol. **67:**7181–7189.
16. **Dore, I., E. Weiss, D. Altschuh, and M. H. V. V. Regenmortel.** 1988. Visualization by electron microscopy of the location of tobacco mosaic virus epitopes reacting with monoclonal antibodies in enzyme immunoassay. Virology **162:**279–289.
17. **French, R., and P. Ahlquist.** 1987. Intercistronic as well as terminal sequences are required for efficient amplification of brome mosaic virus RNA3. J. Virol. **61:**1457–1465.
18. **French, R., M. Janda, and P. Ahlquist.** 1986. Bacterial gene inserted in an engineered RNA virus: efficient expression in monocotyledonous plant cells. Science **231:**1294–1297.
19. **Friedman, R. M., J. G. Levin, P. M. Grimley, and I. K. Berezesky.** 1972. Membrane-associated replication complex in arbovirus infection. J. Virol. **10:**504–515.
20. **Froshauer, S., J. Kartenbeck, and A. Helenius.** 1988. Alphavirus RNA replicase is located on the cytoplasmic surface of endosomes and lysosomes. J. Cell Biol. **107:**2075–2086.
21. **Fuller-Pace, F. V., and P. J. Southern.** 1989. Detection of virus-specific RNA-dependent RNA polymerase activity in extracts from cells infected with lymphocytic choriomeningiris virus: in vitro synthesis of full-length viral RNA species. J. Virol. **63:**1938–1944.
22. **García-Blanco, M. A., D. D. Miller, and M. P. Sheetz.** 1995. Nuclear spreads. I. Visualization of bipartite ribosomal RNA domains. J. Cell Biol. **128:**15–27.
23. **Gething, M.-J., and J. Sambrok.** 1992. Protein folding in the cell. Nature (London) **355:**33–45.
24. **Grimley, P. M., I. Berezesky, and R. M. Friedman.** 1968. Cytoplasmic structures associated with an arbovirus infection: loci of viral ribonucleic acid synthesis. J. Virol. **2:**1326–1338.
25. **Haas, I. G.** 1994. BiP (GRP78), an essential hsp70 resident protein in the endoplasmic reticulum. Experientia **50:**1012–1020.
26. **Hardy, S. F., T. L. German, S. L. Loesch-Fries, and T. C. Hall.** 1979. Highly active template-specific RNA-dependent RNA polymerase from barley leaves infected with brome mosaic virus. Proc. Natl. Acad. Sci. USA **81:** 4956–4960.
27. **Harlow, E., and D. Lane.** 1988. Antibodies, a laboratory manual, p. 53–138. Cold Spring Harbor Laboratory, Cold Spring Harbor, N.Y.
28. **Haseloff, J., P. Goelet, D. Zimmern, P. Ahlquist, R. Dasgupta, and P. Kaesberg.** 1984. Striking similarities in amino acid sequence among nonstructural proteins encoded by RNA viruses that have dissimilar genomic organization. Proc. Natl. Acad. Sci. USA **81:**4358–4362.
29. **Hatta, T., and R. I. B. Francki.** 1981. Cytopathic structures associated with tonoplasts of plant cells infected with cucumber mosaic and tomato aspermy viruses. J. Gen. Virol. **53:**343–346.
30. **Hershberger, R. P.** Personal communication.
31. **Ishikawa, M., J. Díez, A. O. Noueiry, and P. Ahlquist.** Unpublished results.
32. **Jackson, D. A., A. B. Hassan, R. J. Errington, and P. R. Cook.** 1993. Visualization of focal sites of transcription within human nuclei. EMBO J. **12:** 1059–1065.
33. **Janda, M., and P. Ahlquist.** 1993. RNA dependent replication, transcription, and persistence of brome mosaic virus RNA replicons in *S. cerevisiae*. Cell **72:**961–970.
34. **Janda, M., R. French, and P. Ahlquist.** 1987. High efficiency T7 polymerase synthesis of infectious RNA from cloned brome mosaic virus cDNA and effects of 5′ extensions on transcript infectivity. Virology **158:**259–262.
35. **Kao, C., and P. Ahlquist.** 1992. Identification of the domains required for the direct interaction of the helicase-like and polymerase-like RNA replication proteins of brome mosaic virus. J. Virol. **66:**7293–7302.
36. **Kao, C. C., R. Quadt, R. P. Hershberger, and P. Ahlquist.** 1992. Brome mosaic virus RNA replication proteins 1a and 2a form a complex in vitro. J. Virol. **66:**6322–6329.
37. **Kiberstis, P. A., L. S. Loesch-Fries, and T. C. Hall.** 1981. Viral protein synthesis in barley protoplasts inoculated with native and fractionated brome mosaic virus RNA. Virology **112:**804–808.
38. **Kim, K. S.** 1977. An ultrastructural study of inclusions and disease in plant cells infected with cowpea chlorotic mottle virus. J. Gen. Virol. **35:**535–543.
39. **Kroner, P., D. Richards, P. Traynor, and P. Ahlquist.** 1989. Defined mutations in a small region of the brome mosaic virus 2a gene cause diverse temperature-sensitive RNA replication phenotypes. J. Virol. **63:**5302–5309.
40. **Kroner, P. A., B. M. Young, and P. Ahlquist.** 1990. Analysis of the role of brome mosaic virus 1a protein domains in RNA replication, using linker insertion mutagenesis. J. Virol. **64:**6110–6120.
41. **Kunkel, T. A., J. D. Roberts, and R. Zakour.** 1987. Rapid and efficient site-specific mutagenesis without phenotypic selection. Methods Enzymol. **154:**367–382.
42. **Laurière, M., C. Laurière, M. J. Chrispeels, K. D. Johnson, and A. Sturm.** 1989. Characterization of a xylose-specific antiserum that reacts with the complex asparagine-linked glycans of extracellular and vacuolar glycoproteins. Plant Physiol. **90:**1182–1188.
43. **Loesch-Fries, L. S., and T. C. Hall.** 1980. Synthesis, accumulation and encapsidation of individual brome mosaic virus RNA components in barley protoplasts. J. Gen. Virol. **47:**323–332.
44. **Martelli, G. P., and M. Russo.** 1986. Virus-host relationships—symptomatological and ultrastructural aspects, p. 163–205. *In* R. I. B. Francki (ed.), The plant viruses—polyhedral virions with tripartite genomes, 1st ed., vol. 1. Plenum Press, New York.
45. **Martín, M. T., and J. A. García.** 1991. Plum pox potyvirus RNA replication in a crude membrane fraction from infected *Nicotiana clevelandii* leaves. J. Gen. Virol. **72:**785–790.
46. **Miller, W. A., and T. C. Hall.** 1983. Use of micrococcal nuclease in the purification of highly template dependent RNA-dependent RNA polymerase from brome mosaic virus-infected barley. Virology **125:**236–241.
47. **Molla, A., A. V. Paul, and E. Wimmer.** 1993. Effects of temperature and lipophilic agents on poliovirus formation and RNA synthesis in a cell-free system. J. Virol. **67:**5932–5938.
48. **Motoyoshi, F., J. B. Bancroft, J. W. Watts, and J. Burgess.** 1973. The infection of tobacco protoplasts with cowpea chlorotic mottle virus and its RNA. J. Gen. Virol. **20:**177–193.
49. **Munro, S., and H. R. B. Pelham.** 1986. An hsp70-like protein in the ER: identity with the 78 kD glucose-regulated protein and immunoglobulin heavy chain binding protein. Cell **46:**291–300.
50. **Nash, P. D., M. Opas, and M. Michalak.** 1994. Calreticulin: not just another calcium-binding protein. Mol. Cell. Biochem. **135:**71–78.
51. **Pedrazzini, E., and A. Vitale.** 1996. The binding protein (BiP) and the synthesis of secretory proteins. Plant Physiol. Biochem. **34:**207–216.
52. **Peränen, J., P. Laakkonen, M. Hyvönen, and L. Kääriänen.** 1995. The alphavirus replicase protein nsP1 is membrane-associated and has affinity to endocytic organelles. Virology **208:**610–620.
53. **Pombo, A., J. Ferreira, E. Bridge, and M. Carmo-Fonseca.** 1994. Adenovirus replication and transcription sites are spatially separated in the nucleus of infected cells. EMBO J. **13:**5075–5085.
54. **Quadt, R., M. Ishikawa, M. Janda, and P. Ahlquist.** 1995. Formation of brome mosaic virus RNA-dependent RNA polymerase in yeast requires co-expression of viral proteins and viral RNA. Proc. Natl. Acad. Sci. USA **92:**4892–4896.
55. **Quadt, R., and E. M. J. Jaspars.** 1990. Purification and characterization of brome mosaic virus RNA-dependent RNA polymerase. Virology **178:**189–194.
56. **Quadt, R., C. C. Kao, K. S. Browning, R. P. Hershberger, and P. Ahlquist.** 1993. Characterization of a host protein associated with brome mosaic virus RNA-dependent RNA polymerase. Proc. Natl. Acad. Sci. USA **90:**1498–1502.
57. **Quadt, R., H. J. M. Verbeek, and E. M. J. Jaspars.** 1988. Involvement of a nonstructural protein in the RNA synthesis of brome mosaic virus. Virology **165:**256–261.
58. **Rose, M. D., L. M. Misra, and J. P. Vogel.** 1989. KAR2, a karyogamy gene, is the yeast homolog of the mammalian BiP/GRP78 gene. Cell **57:**1211–1221.
59. **Sakai, F., J. R. O. Dawson, and J. W. Watts.** 1979. Synthesis of proteins in tobacco protoplasts infected with brome mosaic virus. J. Gen. Virol. **42:**323–328.
60. **Smirnyagina, E., N.-S. Lin, and P. Ahlquist.** 1996. The polymerase-like core of brome mosaic virus 2a protein, lacking a region interacting with viral 1a protein in vitro, maintains activity and 1a selectivity in RNA replication. J. Virol. **70:**4729–4736.
61. **van Lent, J., M. Storms, F. van der Meer, J. Wellink, and R. Goldbach.** 1991. Tubular structures involved in movement of cowpea mosaic virus are also formed in infected cowpea protoplasts. J. Gen. Virol. **72:**2615–2623.
62. **Wansink, D. G., W. Schul, I. van der Kraan, B. van Steensel, R. van Driel, and L. de Jong.** 1993. Fluorescent labeling of nascent RNA reveals transcription by RNA polymerase II in domains scattered throughout the nucleus. J. Cell Biol. **122:**283–293.
63. **White, J. G., W. B. Amos, and M. Fordham.** 1987. An evaluation of confocal versus conventional imaging of biological structures by fluorescence light microscopy. J. Cell Biol. **105:**41–48.
64. **Wu, S.-X., P. Ahlquist, and P. Kaesberg.** 1992. Active complete in vitro replication of nodavirus RNA requires glycerophospholipid. Proc. Natl. Acad. Sci. USA **89:**11136–11140.
65. **Yaklich, R. W., and E. M. Herman.** 1995. Protein storage vacuoles of soybean aleurone cells accumulate a unique glycoprotein. Plant Sci. **107:**57–67.
66. **Zhang, G. F., and L. A. Staehelin.** 1992. Functional compartmentation of the Golgi apparatus of plant cells. Plant Physiol. **99:**1070–1083.